INSULATION AGING MODELS

Aging of an insulating material or system consists of an irreversible change of physical properties due to action of one or more stresses and/or factors of influence. Aging primarily affects insulation life, where life is intended as time to reach a limit value of specific properties beyond which the insulating material or system is not any longer able to work according to prescribed specifications. For example, if stress is electric field and the property electric strength, life can coincide with insulation breakdown (failure) or time to a given reduction of electric strength.

Aging results, therefore, in a failure rate increasing with stress magnitude and time (1, 2). Typical stresses which cause aging of insulation, possibly until breakdown, are electrical and mechanical stress. Temperature gives rise to thermal stress, which causes changes of properties, thus aging, but does not lead to insulation breakdown. For this reason, temperature is sometimes considered a factor of influence rather than a stress. Another factor of influence is, for example, environmental conditions.

Life is associated to failure probability, since failure must be seen as a stochastic phenomenon (due to several reasons, e.g., intrinsic dishomogeneities of insulating materials and systems, variable environmental conditions, manufacturing processes).

Under the assumption that aging rate, R, does not depend on time, the general aging equation, relating stress, diagnostic property, and aging time can be expressed by (2, 3)

$$A = f(p) = \int_0^t R[S(t')]dt' \qquad (1)$$

where A is aging function (degree of aging), p a diagnostic property (in relative value), S a generic stress or combination of stresses, and t time. If stress is constant, the relationship between aging and life, L, can be formalized as

$$A = A_L(t/L) \qquad (2)$$

where A_L is aging limit, corresponding to the acceptable limit value of the diagnostic property, p_L (end point).

From a geometrical point of view, when stresses are simultaneously applied, the aging equation can be represented in a $(N+2)$ dimension space (N is the number of applied stresses). With two stresses, for example, thermal and electrical stresses, the aging equation is represented by a four-dimension object, while life (obtained choosing a limit value for p, i.e. $p = p_L$, thus $t = L$ in Eqs. (1) and (2)) is a surface of axes S_1, S_2, and L. The surface, Fig. 1, has key intersections with planes at constant S_1, S_2, and L, providing life lines at different values of stress and isochronal lines, at given values of life. As an example, Figs. 2,3,4 show the lines obtained intersecting the surface of Fig. 1 where S_1 and S_2 are electrical, E', and thermal, T', stresses, respectively. Hence, Fig. 2 provides the electrical life lines at given values of thermal stress, Fig. 3 the thermal life lines at given values of electrical stress, and Fig. 4 the isochronal lines, for instance, the loci of the couples E', T' corresponding to pre-selected values of life.

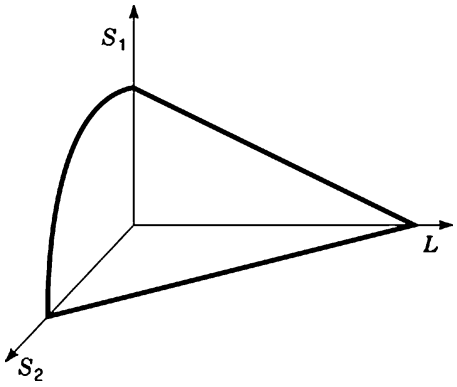

Figure 1. Example of life surface when two stresses, S_1 and S_2, are simultaneously applied (e.g., $S_1 \equiv$ electrical stress and $S_2 \equiv$ thermal stress).

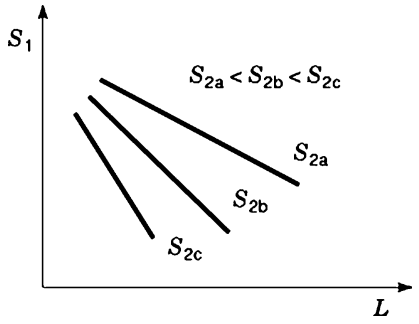

Figure 2. Intersections of the life surface of Fig. 1 with planes at constant thermal stress: electrical life lines at different values of thermal stress ($T' \equiv S_2$).

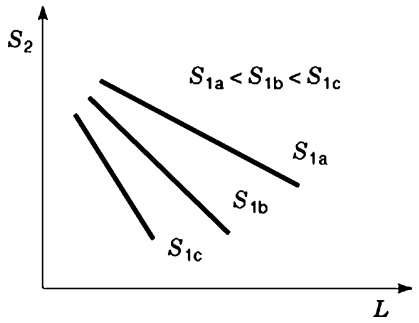

Figure 3. Intersections of the life surface of Fig. 1 with planes at constant electrical stress: thermal life lines at different values of electrical stress ($E' \equiv S_1$).

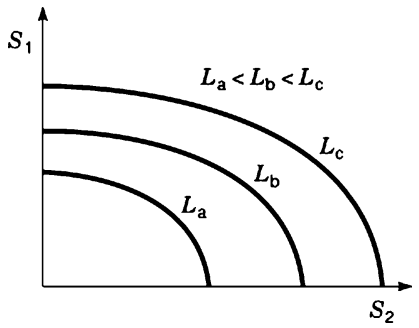

Figure 4. Intersections of the life surface of Fig. 1 with planes at constant life: isochronal lines.

Aging and, in particular, life models are applied to the results of life tests performed at various levels of stress. The purpose is to infer parameters useful for insulation characterization (i.e. the model parameters) and, eventually, predict life at stresses lower than the test ones. While the former goal can be generally reached, the latter requires much more attention. The practice, indeed, of performing life tests at stress values considerably larger than those considered for insulation design (in order to reasonably shorten test times: accelerated testing) does not allow proper evaluation of the life line behavior at low stresses to be carried out. Changes in aging mechanisms can, in fact, invalidate the model holding at high stresses. Hence, the extrapolation usually needed to estimate life at design stresses is based on the unverified assumption of validity of the model which has been selected on the basis of experimental results.

The knowledge of model parameters may provide insights into aging mechanisms; thus, fitting life data by a model could give indication on the processes which cause aging. Prediction, being based upon extrapolation, requires that the simplest model, possibly linear, is searched for. To this aim, the most appropriate coordinate system must be chosen. In general, the lower the number of parameters of a model, the higher is accuracy in estimation of parameters and extrapolated quantities (life, stress). Of course, a compromise is always needed between model complexity and quality of fitting experimental results.

MODELS FOR SINGLE STRESS

Electrical Stress

The simplest empirical models for life under electrical stress are the exponential (*EXP*) and inverse-power (*IP*) models, given by (2, 4):

$$L = L_H \exp[-h(E' - E'_H)] \tag{3}$$

$$L = L_H (E'/E'_H)^{-n} \tag{4}$$

where E_H is the highest value of electrical stress range where the model is thought valid, and L_H is the corresponding time to breakdown, where h and n are the voltage endurance coefficients, respectively. These models provide straight lines in semilog (E vs. log L) or log-log (Log E vs. log L) plots, respectively, and thus have two parameters each: n or h (the reciprocal of slope) and L_H (related to line location). Electrical stress is given by $E' = E - E_0$, being E_0 the value of electrical stress below which electrical aging can be neglected. It is often considered that $E_0 = 0$; thus, electrical stress coincides with electrical field, E.

The model parameters, a function of the other applied stresses (if any), can be estimated by least squares, *LS*, or maximum likelihood, *ML*, procedures, (5, 6), resorting to the results of life tests. As an example, once life tests at M levels of constant electrical stress ($E'_1 > E'_2 > \ldots > E'_M$) have been performed on M samples of insulation specimens, breakdown times are made available. These times are suitably processed [using, in general, the Weibull distribution (5)], so that a chosen life percentile is obtained. The model parameter estimates are achieved, finally, fitting points whose coordinates are electric stress and life percentile: see Fig. 5 (relevant to ethylene-propylene-rubber *EPR*, cable models).

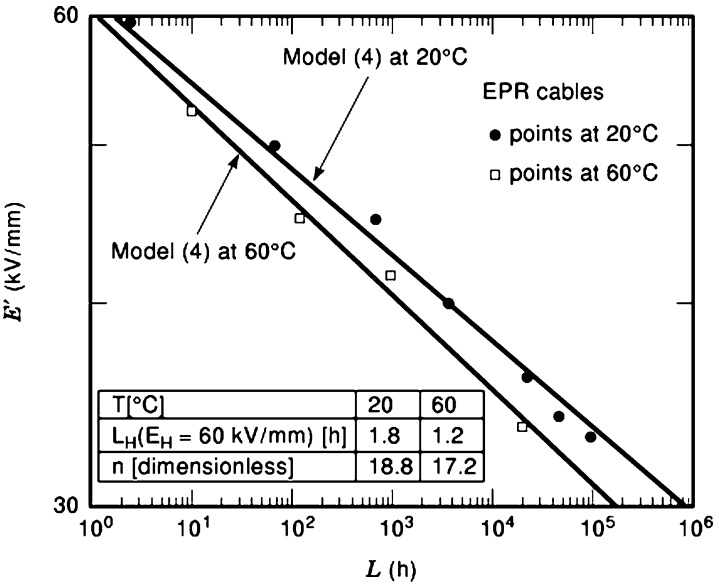

Figure 5. Electrical life lines and experimental life points (failure probability 50%) relevant to EPR aged at 20° and 60°C. Log–log plot. The model parameter values are indicated.

The Weibull distribution of failure times can be written as

$$F(t_F) = 1 - \exp[-(t_F/\alpha)^\beta] \tag{5}$$

where α and β are scale and shape parameters, a function of applied stresses, and t_F is failure time. This function can be linearized in the so-called Weibull plot, having coordinates log ln[1/(1 − F)], log t_F. Once the failure times, t_{Fi}, of each specimen of the tested sample ($i = 1, \ldots, \nu$) associated to their failure probability are reported in this plot, the best fitting line provides an estimate of α and β (least square method), as illustrated in Fig. 6. Life at a given failure percentile, P, is thus obtained from (5) setting $F(t_F) = P$. The least squares method has the advantage of simplicity and graphical output. Several estimators are available for P; among these, the Benard one seems quite simple and accurate (7–9):

$$F(i, \nu) = (i - 0.3)/(\nu + 0.4) \tag{6}$$

Other methods, like ML, can be used to estimate α and β. The choice is a compromise between complexity and accuracy (the latter involves sample size and value of β) (10).

From the observation that α is failure time at probability 63.2%, and thus can be expressed by a best-fitting life model, the possibility comes to write a probabilistic life model, which provides the relationship between stress, failure time, and associated probability (11). This supports the common use of the Weibull distribution to treat electric strength (or breakdown voltage) test data from solid insulating materials (2).

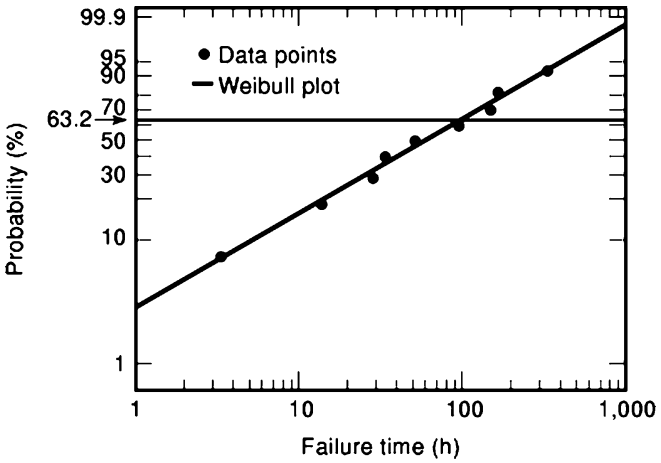

Figure 6. Weibull plot of failure time data obtained from a life test performed on flat specimens of cross-linked polyethylene. Life points and Weibull line.

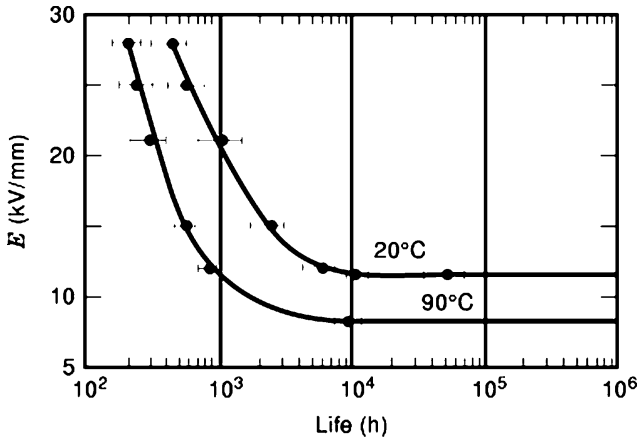

Figure 7. Electrical life lines, at probability 63.2%, derived from the exponential threshold model [Eq. (9)], and life points obtained from tests performed on XLPE cable models at 20° and 90°C [after (18)].

Electric strength tests are generally realized at linearly or step-by-step increasing voltage (12). Testing samples at different rates of voltage rise provides failure times which are related to those that are expected, performing similar tests at constant voltage; thus, Eqs. (3) and (4) may still hold. A relationship between life obtained from increasing-voltage tests, L_P, and constant-voltage tests, L, based on Eq. (4) is (2, 13):

$$L_P = L(n+1) \tag{7}$$

Other expressions are obtained changing life models or the way to increase voltage (14).

Equations (3) and (4) can also take into account the dependence of life on supply-voltage frequency, f, multiplying the right term by f^{-x}, where x is a constant depending on the degradation mechanism, generally <1 (13–17).

Often the results of life tests (life points) do not fit the above linearized models, particularly at low stresses. A typical behavior at low stresses, consisting of lives much longer than those expected on the basis of Eqs. (3) and (4), is associated to the concept of threshold. The electrical threshold indicates the lowest value of electrical field below which life can be considered as mathematically tending to infinity; this practically coincides with a life line presenting an upward curvature and asymptotic behavior to threshold: see Fig. 7 (18). As pointed out by Fig. 7, the threshold value is a function of the other applied stresses, decreasing as these stresses increase. Therefore, an insulation can show electrical life lines with threshold at, for example, low temperature, while showing straight lines, or even life lines with downward curvature at low stresses, as temperature increases (19).

Both EXP and IP models can be modified to account for threshold (2–4). From Eqs. (3) and (4), it derives:

$$L = L_H[(E - E_T)/(E_H - E_T)]^n \tag{8}$$

$$L = L_H \exp[-h(E = E_H)]/[(E - E_T)(E_H - E_T)]^\mu \tag{9}$$

where E_T is the electrical threshold, and μ is a shape factor. An example of application of Eq. (9) is given in Fig. 7, referring to electrical life tests at 20° and 90°C performed on cross-linked Polyethylene (*XLPE*) cable models (18).

The above equations can be applied generally in defined ranges of stresses. The same equation, in fact, may not cover the whole electrical stress range from high to low test stresses, down to design stress, as a consequence of possible changes of the predominant aging mechanism.

Life models derived from investigation of electrical-field induced degradation processes in insulating materials and systems are available in literature. They describe mainly phenomena occurring at high fields, where damage is associated with injection of high-energy electrons, able to break molecular bonds.

A model based on field emission, which relates the electrical tree inception time, t_I, to the local field, E, was proposed by Tanaka and Greenwood (15). The model assumes that charges injected into the insulation (or extracted) contribute to tree initiation only when their cumulative energy exceeds a critical level, C. A limit value of energy below which the injected electrons cannot contribute to insulation degradation, for example, due to trapping phenomena or insufficient energy to break molecular bonds, is considered, which corresponds to an electrical threshold, E_T. The expression of energy as a function of electrical field is given by the Fowler-Nordheim Eq. (20). Accordingly, it results

$$t_I = C'[\exp(-B\Phi^{3/2}/E) - \exp(-B\Phi^{3/2}/E_T)]^{-1} \tag{10}$$

where $C' = C/A$, B and A are material constants, Φ is the effective work function of the injecting electrode. In Eq. (10), t_I does not coincide, in principle, with life, since time to failure in a polymeric insulation is composed by induction time of electrical treeing (from time zero of stress application to tree inception) and tree growth time. However, depending on the type of material and stress magnitude, t_I may approximately coincide with life, L, when tree-growth time is negligible with respect to induction time or, otherwise, if the failure criterion considered for insulation time is tree inception instead of electrical breakdown.

The whole description of lifetime can be achieved adding to t_I the growth time, t_G. A model valid for initiation and

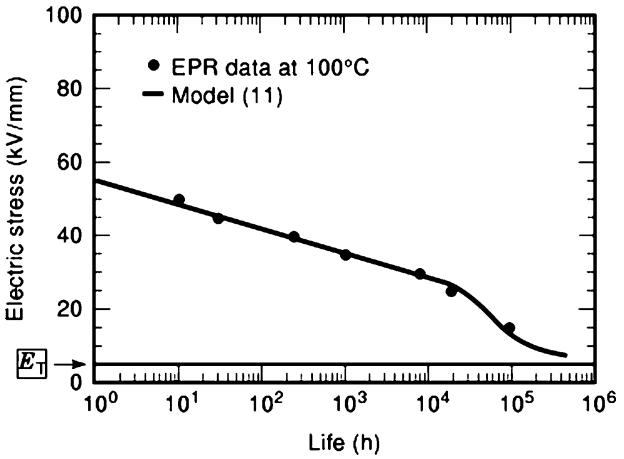

Figure 8. Electrical life line, at probability 50%, derived from model (11), and life points obtained from tests performed on EPR cable models at 90°C [after (19)].

growth of electrical trees in polymeric insulation for cables (e.g., cross-linked Polyethylene, XLPE, and Ethylene-Propylene rubber, EPR) is that proposed in (21). It assumes that local stress enhancements, which can take place in insulation due to, for example, contaminants or protrusions, cause inception of partial discharges in adjacent small cavities ($\approx$10 μm) once the electric field exceeds a threshold value, E_T. Electric charges thus penetrate into the insulation giving rise to channels which develop prevailingly in the electric field direction, forming the electrical tree and leading, ultimately, to breakdown. The resulting model is:

$$t_G = \frac{1}{f b_1 \{\exp[b_2(E - E_T)] - 1\}[\exp(b_3 E + b_4)]} \tag{11}$$

where b_1, b_2, b_3, and b_4 are constants which depend upon material, temperature, and geometry. These constants, besides E_T, constitute five parameters of the model, which is qualitatively plotted in Fig. 8 [the fit is relevant to data obtained for EPR cable models electrically aged at 100°C (19)].

The same physical mechanism promoting tree growth led to another model which includes explicitly fractal dimension of tree, d (22):

$$t_G = S_C(1/2f)N_C\{[\exp(L_b\alpha(E))] - 1\}^{-1} \tag{12}$$

where S_C is the number of tree branches at failure (end point), N_C is a parameter related to material, L_b is tree-branch length, and α is primary ionization coefficient of the Townsend avalanche model. Depending on the α versus E relationship, the model can have four or more parameters, and thus, different life characteristics (with or without threshold) can be obtained from Eq. (12). Moreover, even variation of fractal dimension with growth time can be taken into account (improving fitting and/or the range of model validity), but this would increase further on the parameter number.

Quite similar is the approach proposed in (23), where the charge amount generated by partial discharges and/or penetration depth are considered as the diagnostic properties. The following aging equation is proposed:

$$Q_i = k_1\{\exp[k_2(E - E_T)^b t^{(1/d)}] - 1\} \tag{13}$$

where Q_i is the amount of charge flowing in the channels with penetration depth x_i; k_1, k_2 and b are coefficients depending on material and tree-growth phenomenology, E_T is the threshold, the limit value of electrical stress below which tree does not grow. The property charge amount can be turned into penetration depth by the following relationship:

$$Q_i = k_1[\exp(k_3 x_i) - 1] \tag{14}$$

so that the equation can be applied to the most convenient recorded property. Once an end point for Q_i or x_i (i.e., Q_m or x_m) is selected, the life model derived from Eq. (13) becomes

$$t_G = \frac{\{\ln[Q_m/k_1) + 1]\}^d}{k_4(E - E_T)} \tag{15}$$

where $k_4 = k_3 k^{(1/d)}{}_2$. This model has the same structure of Eq. (8), being characterized by the same number of parameters (function of the applied stresses other than the electrical one). Like Eq. (8), it can be used as a phenomenological tool to fit tree growth data, even if the electrical tree does not exhibit a fractal dimension; in this case, its parameters can lose any physical meaning.

Finally, it is worthwhile mentioning that Eq. (8) is practically coincident with that obtained by Dakin and Studniartz (24) for breakdown due to surface discharges.

Another aging model, valid for electrical degradation which affects the diagnostic property electric strength, E_S, is (2, 3):

$$1 - (E_S/E_{S0})^{(n+1)} = (E/E_{S0})^n t/t_0 \tag{16}$$

where E_{S0} and t_0 are electric strength and corresponding time to breakdown measured on unaged specimens. Fixing the end point $E_S = 0$, Eq. (16) provides life model (4). A similar approach, however, can be followed for other life models.

Thermal Stress

The Arrhenius model, based on reaction rate theory, is generally used as thermal life model (35):

$$L = L_0 \exp(-BT') \tag{17}$$

where T' is thermal stress, defined as $T' = (1/T_0) - (1/T)$, T is absolute temperature, T_0 is a lower limit temperature below which thermal aging is negligible for the degradation reaction prevailing in the range of interest, L_0 is the life at temperature T_0, and $B = A_E/k$ (A_E is the activation energy of the degradation process; k is the Boltzmann constant). Life is intended as the time to reach a fixed limit (end point) of a diagnostic property.

This model provides a straight life line in the coordinate system ln L vs. T' [or ln L vs. $(1/T)$], as it is shown in Fig. 9 (where the model is applied to data obtained from Polybutylene Therephthalate (30% glass filled) specimens and diagnostic property tensile strength). Based on this line, the IEC Standard (25) establishes the figures for thermal

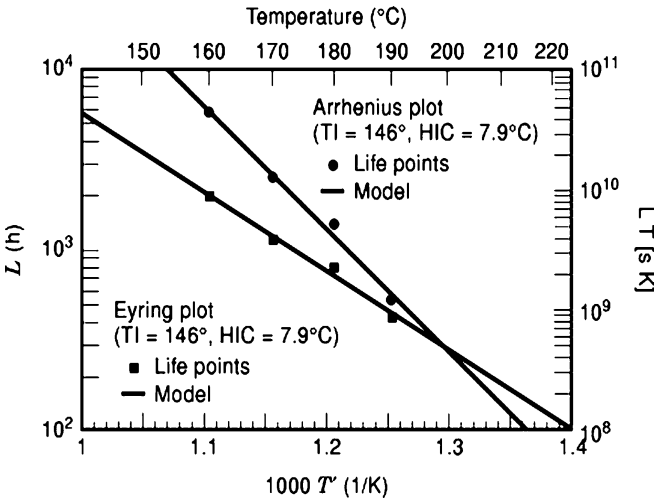

Figure 9. Thermal endurance graphs obtained by the Arrhenius and Eyring models. The life points (mean values of time to end point) are relevant to Polybutylene Therephthalate, 30% glass filled; the values of TI and HIC are reported.

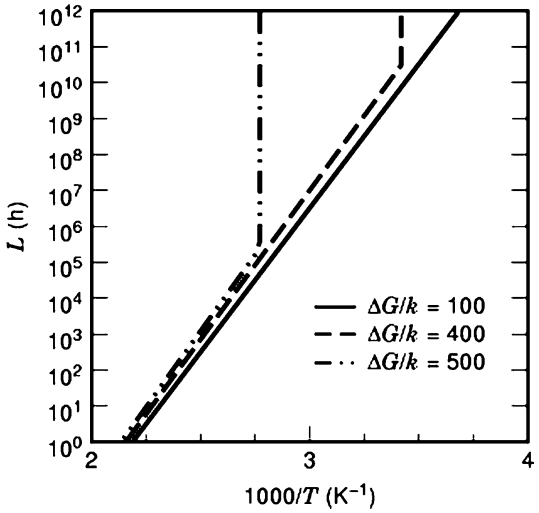

Figure 10. Thermal life lines, according to Eq. (20), for different values of $\Delta G/k$ [after (32)].

endurance characterization, that is, temperature index (*TI*) and Halving Interval in Celsius degrees (*HIC*). The former is the temperature, in Celsius degrees, derived from the thermal endurance relationship at a given time, for example, 20,000 h. The latter is the temperature interval in Celsius degrees, which expresses the halving of the time to end point taken at the temperature of the TI.

An alternative to Eq. (17), the Eyring model, is sometimes recommended (26). It is given by (27):

$$L = (A_L h/kT)\exp(\Delta G^{\#}/kT) \tag{18}$$

where h is the Planck constant, A_L is a parameter related to the chosen property end point, and $\Delta G^{\#}$ is the activation free energy ($\Delta G^{\#} = G_a - G_1$ is the height of the energy barrier, G_1 and G_a being the free energies of reactant ground and activated states, respectively). A_L can be expressed as a function of the activation entropy, ΔS, as, for example, $A_L \propto \exp(-\Delta S/k)$ (28, 29) which can also take into account the contribution of free motion produced by quantum wells and viscosity, often nonnegligible in liquids and solids. The model can be linearized in $\log(LT)$ vs. $(1/T)$ plot, thus providing the same indices of Eq. (17). Even if this model provides a background exploited for multistress life modeling, it does not give, generally, significant improvements, regarding the quality of data fitting, in thermal endurance, due to the quite narrow ranges of test and extrapolation stresses (see, e.g., Fig. 9) (30).

A linear relationship between activation enthalpy, ΔH, and entropy, ΔS (which define the free energy according to $\Delta G = \Delta H - T\Delta S$), was noticed (31). It gives rise to a correlation between the logarithm of the preexponential term and activation energy [Eq. (17)] or enthalpy [Eq. (18)]. This affects thermal life models: the Arrhenius model becomes, for example, (4, 30):

$$L_T = L_0 \exp[-T'(k_5 \log L_0 + k_6)] \tag{19}$$

with one more parameter with respect to Eq. (17).

Threshold can also be considered for thermal aging. If reversibility of degradation reactions is assumed, an expression for thermal life where thermal threshold appears can be obtained (32):

$$L = (K_f + K_b)^{-1} \ln\left\{\frac{1+\exp[\Delta G/(kT_T)]}{\exp[\Delta G/(kT_T)] - \exp[\Delta G/(kT)]}\right\} \qquad T \geq T_T \tag{20}$$

$$L = \infty \qquad T \leq T_T \tag{21}$$

where K_f and K_b are forward and backward reaction rate constant [given by A_L/L, Eq. (18)], $\Delta G = G_2 - G_1$ (G_2 is the free energy of the product state), and T_T is thermal threshold. Figure 10 shows examples of life lines obtained from Eq. (20) (32).

A simpler phenomenological approach introduces the threshold in the Arrhenius equation in the same way as for the electrical exponential life threshold model, Eq. (9), that is (4, 28)

$$L = L_0[\exp(-BT')]/[(T'/T'_T) - 1]^{\mu} \tag{22}$$

where the three parameters, B, T_T, and μ, are functions of the other applied stresses (as it holds, in general, also for the above thermal life models).

Mechanical Stress

An empirical model often employed to fit data from mechanical stress aging tests resorts to the inverse-power relationship, and thus is similar to Eq. (4) (4):

$$L = L_H(M'/M'_H)^{-m} \tag{23}$$

where $M' = M - M_0$ is mechanical stress (either constant or cyclic), m is the endurance coefficient, and M'_H and L_H have the same meaning as in Eq. (4). As for electrical aging, a threshold model can be obtained from Eq. (23), which corresponds to Eq. (8), for instance,

$$L = L_H[(M - M_T)/(M_H - M_T)]^{-m} \tag{24}$$

where M_H is the mechanical threshold.

MODELS FOR MULTISTRESS

A general approach to multistress phenomenological models, holding when stresses are simultaneously applied, can consist of multiplication of aging rates, corrected by a term which takes into account synergism among stresses (2, 33). Henceforward, multistress life is given by:

$$L/L_0 = (L_1/L_0)(L_2/L_0)\ldots, (L_P/L_0)G(S_1, S_2, \ldots, S_P) \quad (25)$$

where $L_1, \ldots, L_P$ are lives under stresses $S_1, \ldots, S_P$ singly applied (L_0 is a normalization life), and G is the corrective term. The models for electrical, thermal, and mechanical stress described above can, in principle, be included in Eq. (25), taking care of compatibility conditions (e.g. $L/L_0 = L_1/L_0$ for $S_2 = \cdots = S_P = 0$). Other factors of influence, as environmental factors, could be considered in the framework of model Eq. (25), but this is still a matter of investigation. With evaluation of synergistic effects and the relevant expression, possible changes of aging mechanisms (thus aging rate) with time can complicate considerably the problem of explication of Eq. (25).

Thermoelectrical Life Models

According to Eq. (25), and considering either the exponential or the inverse-power model (Eqs. (3), (4)) for life under electrical stress, and the Arrhenius model for thermal life [Eq. (17)], the following expressions for combined thermoelectrical life were obtained (2, 4):

$$L = L_0 \exp(-BT' - hE' + bE'T') \quad (26)$$

$$L = L_0 (E/E_0)^{-(n-bT')} \exp(-BT') \quad (27)$$

These models are characterized by four parameters, namely, L_0, h or n, B and b. The last belongs to the corrective term, and thus gives information on stress synergism. Both models Eqs. (26) and (27) provide a life surface like that of Fig. 1, with intersections given by Figs. 2,3,4, in appropriate coordinate systems [i.e., $\ln L, E', T'$ for model Eq. (26); $\ln L, \log(E/E_0), T'$ for model Eq. (27)]. Once the parameters have been estimated [by accelerated electrical, thermal, and multi-stress tests (19)], life can be determined for any pair of values of E' and T' in the model validity range.

Also the threshold models can be accommodated in Eq. (25), even if compatibility and boundary conditions are slightly more complex. Referring to electrical and thermal life models like Eqs. (9) and (22), the thermoelectrical life model becomes (4, 28):

$$L = K_0 L_0 \frac{\exp(-hE' - BT' + bE'T')}{[E'/E'_{T0} + T/T_{T0} - 1]^{\mu}} \quad (28)$$

where E'_{T0} and T'_{T0} are electrical and thermal threshold for $T' = 0$ and $E' = 0$, respectively, and K_0 is a normalization parameter.

Equation (28) is represented by the life surface plotted in Fig. 11. It is noteworthy that the electrical life lines show a threshold decreasing to zero as T' increases. The same holds for thermal life lines when considering the variation of thermal threshold with E'.

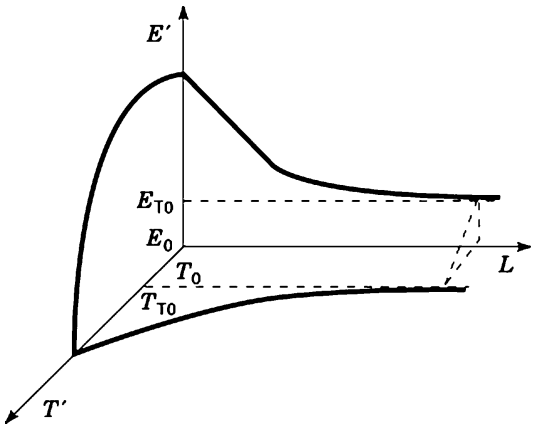

Figure 11. Life surface under thermoelectrical stress for threshold life model [Eq. (28)].

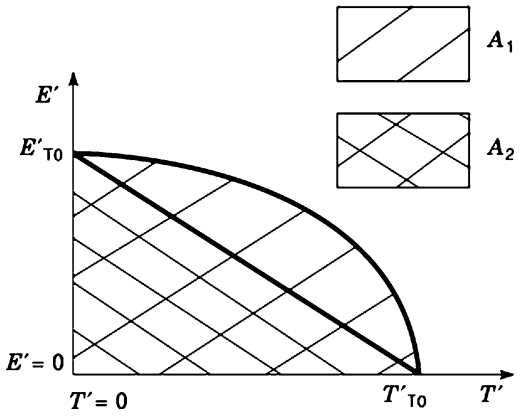

Figure 12. Isochronal threshold line (Fig. 11) and definition of SCI [Eqs. 29–34].

A general model was proposed in (34), which can fit data exhibiting both linear and threshold life behavior, that is, encompassing both Eq. (26) and Eq. (28):

$$L = L_0 \frac{\exp(-hE' - BT' + bE'T')}{[E'/E'_{T0} + T/T_{T0} - k_c(T/T_{T0})(E'/E'_{T0}) - 1]^{\mu(E',T')}} \quad (29)$$

with

$$\mu(E', T') = \left[\frac{(E' - E'_{T0})^2}{E'^2_{T0}} + \frac{(T' - T'_{T0})^2}{T'^2_{T0}} \right] \quad (30)$$

$$k_C = 2(1 - 1/\mathrm{SCI}) \quad (31)$$

SCI is the stress compatibility index, which is given by the ratio between the area defined by the threshold isochronal line and that of the triangle connecting the axes intersections of the isochronal line and the origin, i.e. A_1/A_2 of Fig. 12. The SCI can be associated to n, E_H (or electric strength, E_S), TI, HIC to complete the endurance characterization of an insulation under thermoelectrical stress.

Thermoelectrical life models were also derived resorting to physical approaches based on the Eyring or Arrhenius relationships.

The common feature is that the activation energy [Eq. (17)] or enthalpy [Eq. (18), considering that $\Delta G = \Delta H - T\,\Delta S$] is lowered by a term function of electrical stress.

From the Arrhenius relationship, the following models were presented for thermoelectrical life lines without and with threshold (24–36):

$$L = k_7 \exp(-BT' - b_1 T' E') \tag{32}$$

$$L = [Cf(E - E_T)]^{-1} \exp[-BT' - b_1 T' E'] \tag{33}$$

where C is the fraction of electrons reaching the most critical site, and $b_1 E'$ is the contribution of electrical field in lowering the activation energy of thermal degradation reaction. These models, however, do not comply with the compatibility condition that $L = L_E$ for $T' = 0$ (L_E is life under electrical stress).

Total compatibility is achieved by the approach presented in (37), based on the Eyring law. Life is given by

$$L = (k_3 h/kT) \exp[-BT' - (k_9 - k_{10} T') f(E)] \tag{34}$$

It was shown in (33) that considering the following expressions for $f(E)$:

$$f(E) = E' \tag{35}$$

$$f(E) = \ln(E/E_0) \tag{36}$$

models having the same form of Eqs. (26) and (27) are obtained (once the temperature dependence of the preexponential term in Eq. (34) has been neglected). Moreover, in (28) it is shown that parameter k_8 of Eq. (34) is proportional to $\exp(-\Delta S)$. These observations establish a close connection between phenomenological models like Eq. (26), Eq. (27) and physical models based on a thermodynamic approach.

The experimental evidence, provided by some materials and insulations systems, of upward curvature of life lines (tendency to threshold) was approached considering partially reversible reactions both in (16, 38) and (29, 32).

The model proposed in (16, 38) is

$$L \propto (h/2kT) \exp(\Delta G/kT) \operatorname{csch}(e\delta E/kT) \tag{37}$$

where δ is the width of the energy barrier, and e is the electronic charge accelerated by electric field, E, so as to gain mean energy $e\delta E$. Equation (37) simplifies for high electrical stresses, where aging reaction goes prevailingly in the forward direction, to an exponential model similar to (32). Therefore, Eq. (37) provides electrical life lines at a chosen temperature, in semilog plot, which are straight at high stresses but tend to infinite life when electrical stress approaches zero. δ, called "scattering distance," is related to microstructural characteristics of the material (e.g., the dimensions of the amorphous regions between crystalline lamellas in Polyethylene) and is temperature dependent (39). A relation between δ and the formation of submicrocavities in the material, due to breakdown of weak bonds (caused by electrons accelerated by the field), was proposed (39). Due to the lack of appropriate analytical relationships, the model is not fully defined as a function of temperature and time, and thus cannot be properly considered a multistress model: it can fit experimental results derived from electrical life tests at chosen temperatures, like Eq. (9), but cannot be used to infer material behavior at temperatures different from the test ones. It must be noted that breakdown in most insulation systems is due to imperfections (e.g., protrusions, contaminants, voids in polymeric insulations) (40, 41). Therefore, any physical model should be applied locally knowing the real electric field inside the insulation.

At fields close to those considered for insulation design, in homogeneous polymeric insulating materials (to which technology is tending due to material performance improvement), it is unlikely that free electrons can acquire enough energy to break even weak bonds. Therefore, in (29–43) the effect of trapped space charges, for instance, charges steadily present into insulation with very small mobility, is focused. The limit condition for electrical aging has been addressed to the presence of trapped space charges which store electromechanical energy and are able to promote cracks and plastic deformations in the polymer structure. Equation (20), where life is intended as time to formation of cavities or crazes into the insulation, can be considered. When the applied field, superimposed to temperature, is large enough to inject space charges inside the insulation (from electrodes, semiconductor protrusions, etc.), which are trapped in correspondence of defect sites, the initial state free energy, G_1, may be raised by an amount ΔG_m. The latter is proportional to the unit volume electrostatic and electromechanical energy (W_{es} and W_{em}, respectively) which is stored by the space-charge centers. Hence, the term ΔG becomes a function of E:

$$\Delta G(E) = G_2 - [G_1 + \Delta G_m(E)] = G_2 - G_1 - AW_{es} - BW_{em} \tag{38}$$

where A and B are proportionality constants ≤ 1. If the electrostatic energy is not released in the product state, 2, the term AW_{es} disappears in Eq. (38). The contribution of the space charge, q, to the stored electrostatic and electromechanical energies is quantified in (32), resulting in $W_{es} = C_1 q 2$ and $W_{em} = C_2 q^2$ (C_1 and C_2 are proportionality constants), while a simple expression of the dependence of q on the electrical field is $q = C_3 E^a$. This approach holds in the dc regime, since ac aging requires consideration of another term lowering ΔG, which takes into account fatigue (as pointed out further on). The following expression is finally derived for life (29–43):

$$L = \frac{2h}{kT} exp(\Delta S/k) \frac{exp[(DHK - C' E^{2a}/2)/T]}{cosh[(\Delta K - C' E^{2a})/2T]} \{-ln[\frac{A_{eq}(E) - A^*}{A_{eq}(E) - A(0)}]\} \tag{39}$$

where $C' = C_3/k$ is a constant; ΔS, ΔK, and DHK are entropy, free energy, and enthalpy terms; A^* is the fraction of moieties that have to be converted from state 1 to state 2 in order for the insulation life to end; A_{eq} is the equilibrium value of A ($A_{eq} = K_f/(K_b + K_f)$); and $A(0)$ is the initial value of A ($A = c_2/(c_1 + c_2)$, with c_1 and c_2 being the concentration of reacting moieties in states 1 and 2). Equation (39) provides insulation life in a form in which dependence upon electric field and temperature is made fully explicit,

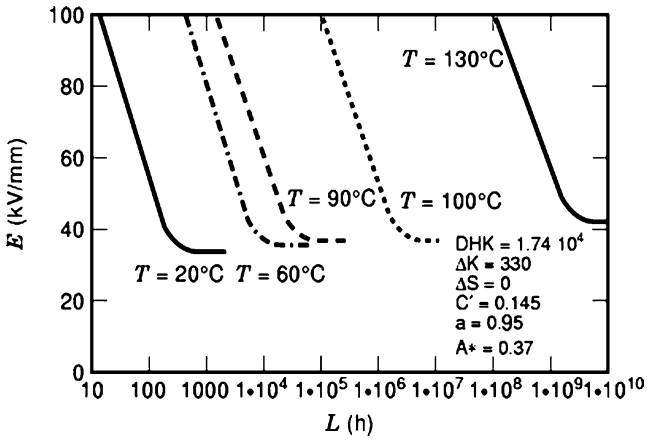

Figure 13. Parametric representation of electrical life lines at different values of temperature, derived from Eq. (39).

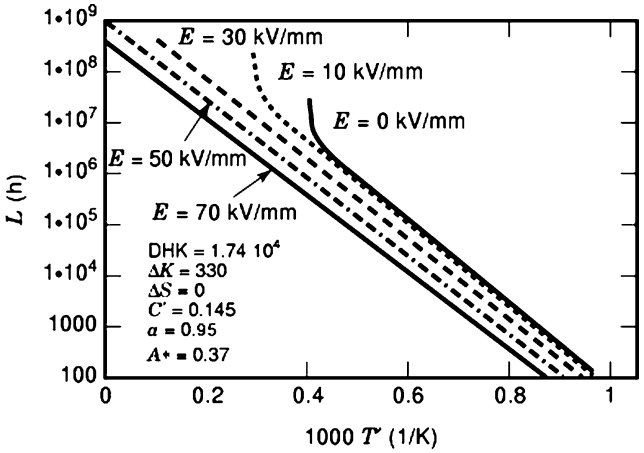

Figure 14. Parametric representation of thermal life lines at different values of electrical field, derived from Eq. (39).

thus enabling the derivation of electrical life lines at different temperatures and of thermal life lines at different values of electrical field. It is characterized by seven parameters, namely, ΔS, DHK, ΔK, a, C', A^*, and $A(0)$, but $A(0)$ can be considered zero (for materials with high level of homogeneity and cleanliness) (29). Hence, the number of parameters can be reduced to six. Equation (39) behaves similarly to the general phenomenological model, Eq. (29). Both models have electrical and thermal thresholds, which vary with E, T, and disappear for electrical and thermal stresses above certain levels. This is displayed in Figs. 13 and 14, where a parametric representation of electrical life lines and thermal life lines at different values of temperature and electrical field, derived from Eq. (39), is reported. It is noteworthy that the electrical life lines may show double curvature (downward at high stresses, upward at low stresses); thus, the model can fit a large amount of data reported in literature. Of course, if data do not comply with the assumptions on which the model is based (in particular, dc aging and life corresponding to time to formation of microcavities), it takes phenomenological validity mainly, and its parameters can lose physical meaning. Results derived applying the model to experimental data obtained from life tests carried out on polyethylene therephtalate (*PET*) films, 36 μm thick, aged at different values of electrical field and temperature, are displayed in Fig. 15 (29).

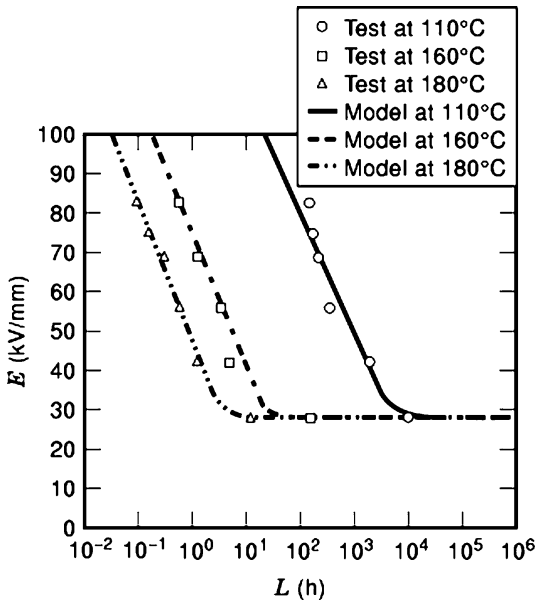

Figure 15. Electrical life lines at different values of temperature, derived from Eq. (39), applied to PET data subjected to thermoelectrical life tests under dc voltage. Experimental life points, at failure probability 63.2%, are also displayed [after (29)].

As previously highlighted, Equation (39) holds in the dc regime. Nevertheless, it can fit ac data as well, see (44). The goal to extend the validity of Eq. (39) to ac regimes can be achieved by accounting for the role of electrical fatigue in the presence of a sinusoidal field, via a proper term to be subtracted from the right-hand side of Eq. (38). By doing so, the life model expressed by Eq. (39) is then characterized by frequency-dependent parameters.

The aging effects of space charges can be amplified by voltage polarity inversions, that may occur in transmission dc cables. It has been proved that such polarity inversions, when associated with the presence of space charge stored inside the insulation thickness, are the prevailing cause of life reduction for polymeric insulation subjected to a dc electrical field (45). Extensive experimental work on PE-based materials led to an expression able to describe life under voltage polarity inversion, that relates the ratio of life without and with polarity inversion, L/L_i, to the maximum field measured in the insulation, E_M, the space charge density, Q, and the exponent s in the time dependence ($Q \propto t^{-s}$) of the charge depletion (46):

$$ln[(L/L_i) - 1] = A_1 + A_2 ln(Q) + A_3 ln(E_M) + A_4 ln(s) + A_5 ln(f) \quad (40)$$

where f is the polarity inversion frequency and A_1, A_2, A_3, A_4, A_5 are coefficients that are function of the type of material. Equation (40) can be simplified by considering the power law dependence of space charge on poling electrical field E, above a characteristic threshold E_T, that is:

$$Q = A_0 E^a \quad (41)$$

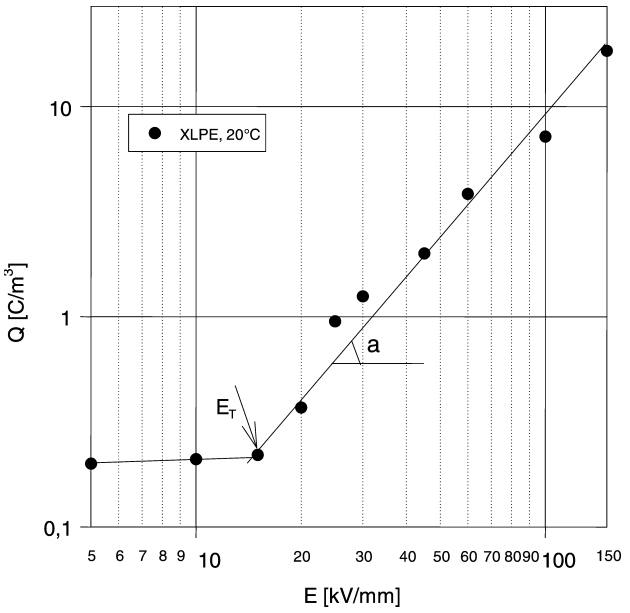

Figure 16. Example of Q vs E characteristic, relevant to XLPE, 20°C. The threshold for space charge accumulation, E_T, is indicated by an arrow.

where the power law exponent a - the same quantity that appears in Eq. (39) - represents the slope of the high-field part of the Q vs E characteristic in a log-log plot. This experimental behavior is illustrated in Fig. 16, where the threshold for charge accumulation, E_T, is indicated by an arrow. Using Eq. (41) together with some other approximations results in the following expression:

$$\ln[(L/L_i) - 1] = b' \ln(KE) + A_5 \ln(f) \tag{42}$$

where K and b' are functions of the coefficients A_0, A_1, A_2, A_3, A_4. Equations (40) and (42) show that the larger the amount of space charge, the shorter is life under voltage polarity inversion with respect to life without inversion.

Notwithstanding the above-mentioned technological improvements, real polymeric insulating materials most often exhibit micro-voids of sizes around a few tens of microns. For this reason, another thermo-electrical life model was derived by considering the effects of charge accumulation at polymer-void interface and injection into the void (47, 48). In this framework, injected charges give rise to hot-electron avalanches that cross the air-filled cavity and collide with the void-polymer interface. Then, hot electrons release their kinetic energy through high-energy scatterings within polymer slabs adjacent to the void surface, thereby damaging the polymer matrix. While breakdown conditions are commonly found within the void, electrons in the polymer are far from breakdown regime and undergo a fast thermalization process. This can occur through two strongly inelastic scattering processes that take place above ~8 eV, i.e. impact ionization and Dissociative Electron Attachment (DEA) of C-H bonds. The latter process causes chemical damage - thus ageing - which accumulates in the polymer as subsequent avalanches travel across the void and impact on the void-polymer interface. In the case of polyolefins, e.g. Polyethylene (PE), chemical damage can be assumed to consist of the breaking of a percentage of CH bonds large enough to cause irreversible ageing.

As argued in (47, 48) on the basis of mean free paths for electron scatterings in polymers, the whole hot-electron cooling process occurs in a slab of thickness D_{dis} 400 Å and the damage growth rate in the insulation, $R_{\rm dis}$, can be derived as a function of void size d, electric field E, and temperature T, as:

$$R_{dis} = D_{dis}/t_{dis} \tag{43}$$

where $t_{\rm dis}$ is the time-to-disruption (i.e. to severe and irreversible chemical degradation) of the slab. $t_{\rm dis}$ can be roughly estimated as the time needed to dissociate half of the CH bonds inside the slab, as follows:

$$t_{dis} = N_{CH}/(2R_{el}F_{eff}F_{hot}) \tag{44}$$

where $N_{\rm CH}$ is the number of CH bonds in the slab, $R_{\rm el}$ is the rate of electrons colliding with the polymer surface after being injected into the void and multiplied by the avalanche mechanism, $F_{\rm hot}$ is the hot-fraction (energy >8 eV) of electrons impinging the polymer surface and $F_{\rm eff}$ is the fraction of hot-electrons that are effective in causing chemical damage through DEA. $F_{\rm hot}$ and $F_{\rm eff}$ can be obtained as a function of field on the basis of the energy distributions of the avalanche-electrons.

Finally, an expression for the life L of the system is obtained by assuming that time-to-failure (life) is the time to the formation of a damaged zone (made of contiguous sequentially-damaged slabs of thickness $D_{\rm dis}$) of critical size $d_{\rm C}$, large enough to start an electrical tree e.g. by enhancing the local field, or, simply, by increasing the volume of damaged polymer. L can be then estimated as follows (47, 48):

$$L = d_C/R_{dis} \tag{45}$$

It was argued in (47, 48) that, with the exception of $d_{\rm C}$, all the parameters that characterize this ageing and life model have a physical meaning, since they are related to physical and chemical properties of the polymer and of the air that fills the void. The only phenomenological parameter of the model is $d_{\rm C}$, that can be guessed either *a-posteriori* by comparing life estimates obtained from Eq. (42) with experimental times-to-failure (through, e.g., tests at fairly high values of field and, hence, lasting relatively short times) or *a-priori* via theoretical considerations. From this respect, the approach developed in (49) can provide a reasonable estimate for $d_{\rm C}$ (growth of a pit of around 1.5/3 μm of length), thereby separating the stage dominated by avalanches in the void from that relevant to tree growth. It is noteworthy that this approach is intimately related to the most effective technique for diagnosis and ageing assessment of electrical insulation systems, that is, partial discharges (PD) measurements. Indeed, electron avalanches in cavities will turn into PD once damage is growing.

Finally, it must be observed that a physical description of degradation and failure of insulating materials should likely refer to a combination of models, depending on stress levels and insulation configuration. Thus, the time to breakdown would result from the sum of the life values provided by each model (50). At relatively high stresses,

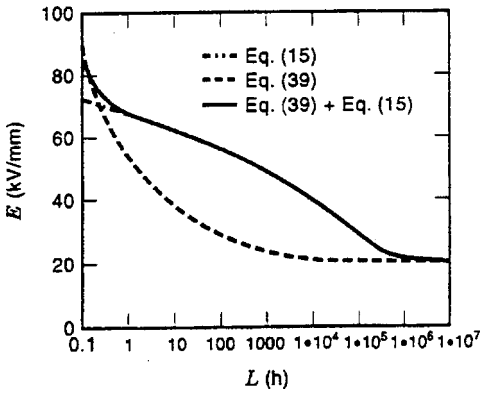

Figure 17. Examples of life curves obtained from combinations of Eqs. (39) and (15).

failure time could be given by the combination of the injection model, Eq. (10), and the tree-growth model, Eq. (15), one prevailing on the other depending on stress level, kind of insulating material, and aging cell (e.g., thermoplastic or thermosetting material, cell at uniform or divergent field). At relatively low stresses and for homogeneous materials, combination of Eqs. (39) and (15) could encompass both tree induction and growth, thus time to breakdown: see, as an example, Fig. 17.

Thermo-Mechanical Life Models

A physical approach based on Arrhenius or Eyring relationships, similar to that presented above for thermoelectrical aging, can hold.

A thermomechanical life model derived from the Arrhenius relationship is (51, 52):

$$L = k_{11}\exp(-B_M T\prime - \tau T' M) \tag{46}$$

where k_{11} is a constant, B_M is related to the activation energy of the fracture process, and τ is the activation volume for submicrocrack formation.

Like (37), a thermomechanical model can be obtained resorting to the Erying law and considering partially reversible degradation reactions, that is (53):

$$L \propto (h/2kT)\exp(\Delta G/kT)csch(\tau M/kT) \tag{47}$$

Equation (47) simplifies to the exponential model [Eq. (46)] (once the temperature dependence of the preexponential term has been neglected) for high mechanical stress. Both models have, however, compatibility problems, since $L \neq L_M$ for $T' = 0$ (L_M is life under mechanical stress). Fully compatible thermomechanical models can be constructed as made above for thermoelectrical stress, Eqs. (26–29,34–36) and (34–36), simply substituting M to E and $M' = M - M_0$ to E', in order that sets of life data either linear or showing threshold can be fitted.

Thermo-Electrical-Mechanical Life Models

A general, phenomenological model with three stresses operating simultaneously can be achieved from Eq. (25), once appropriate expressions for single-stress lives, as well as for the corrective term, have been selected.

Considering the Arrhenius relationship for thermal life and the inverse power law for electrical [Eq. (4)] and mechanical [Eq. (23)] life, the following thermo-electrical-mechanical life model was obtained (4, 54):

$$\begin{aligned} L = L_0 exp\{&-BT' - n[log(E/E_0)] - m[log(M/M_0)] \\ &+ b'T'[log(E/E_0)] + b''T'[log(M/M_0)] \\ &+ b'''T'[log(E/E_0)log(M/M_0)]\} \end{aligned} \tag{48}$$

which is characterized by ten parameters and provides straight life lines in $\log(E/E_0)$, $\log(M/M_0)$, T' vs the log L coordinate system [Eq. (48) can be represented in a four-dimension space; thus, only the intersections with planes at constant stress can be plotted as three-dimension surfaces, e.g. Fig. 1].

A model similar to Eq. (48) can be obtained using exponential relationships for electrical [Eq. (3)] and mechanical life models (4).

PROBABILISTIC APPROACH

The probabilistic models for life inference under single and multiple stresses reported in literature belong, in general, to the class of parametric methods.

A general procedure which allows definition of probabilistic life models, based on the Weibull function [Eq. (5)], is discussed above for electrical stress, but may also hold for multistress (as well as, in general, for any other best-fitting probability distribution).

An example of an application of this procedure can refer to the exponential threshold model [Eq. (9)]. From Eq. (5) and considering for α the expression given by Eq. (9), the following relationship is achieved (11):

$$F(t_F) = 1 - exp\{-[\frac{t_F}{L_H}(\frac{E - E_T}{E_H - E_T})^{\mu}\exp(h(E - E_H))]^{\beta}\} \tag{49}$$

which is a five-parameter model. An application of this model to the results of accelerated life tests performed on XLPE cable models at 20°C is shown in Fig. 18, where the life lines at failure probability 10 and 90%, obtained from Eq. (49), are plotted. Once the model parameters have been estimated, failure times at chosen stresses and probabilities can be derived from a model like Eq. (49).

In principle, any model relating failure time to stress can be used for α, but it must be observed that the distribution of breakdown voltages (or gradients), $F(E)$, which results from, for example, electric strength tests, may not be a Weibull function anymore. For example, Eq. (49) becomes a Gumbel distribution for t_F = constant, which, however, can often fit electric-strength test results quite well.

The shape parameter, β, can be assumed, as a first approximation, constant with stress, and can take the mean value calculated for the whole set of life tests. This assumption generally provides good data fitting (see, e.g., Fig. 18), but may affect the accuracy of the failure time estimates at extreme percentiles (e.g., 95% or 5%). When fitting is not satisfactory, the stress dependence of β can be expressed by linear or curvilinear regressions of the values estimated at each stress level, but in this case, the number of model parameters increases, which may affect the estimates' ac-

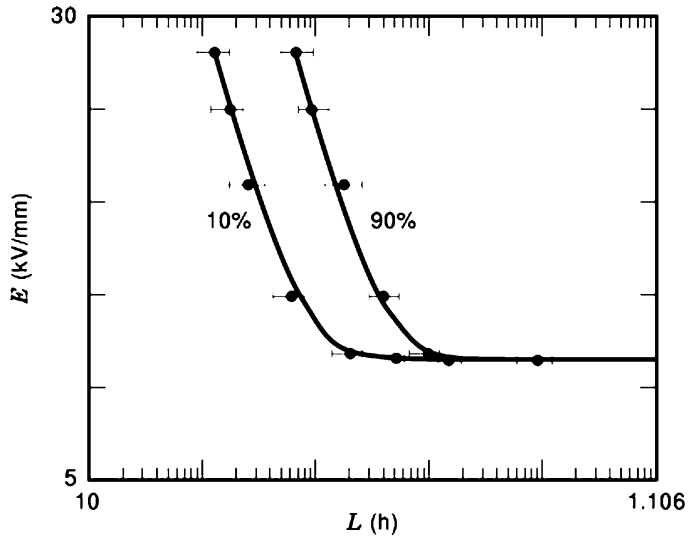

Figure 18. Electrical life lines at probability 10% and 90% derived according to the probabilistic life model, Eq. (43), for XLPE cables aged at 20°C. The confidence intervals of the experimental points are calculated at probability 95% [after (11)].

curacy anyway.

Besides the obvious consideration that failure is a stochastic phenomenon, which must be treated by probabilistic models, the advantage of the probabilistic approach is that the results obtained on test specimens can be extended, for rough evaluations, to more complex situations. The acceptable failure probability, in fact, can be assumed suitably low, considering a safety coefficient which takes into account the risks connected with changes of insulation configuration and working conditions, with respect to the test features, as well as model extrapolation for design-stress estimation.

NONPARAMETRIC AND ADAPTIVE APPROACHES

Nonparametric approaches for life-percentile estimation do not resort to life models. The purpose is, in fact, life prediction, rather than insulation characterization.

A typical procedure of probabilistic nonparametric modeling is the following. Let $V_1, V_2, \ldots, V_K$ denote the test voltage levels ($V_1 > V_2 > V_K$) and $\nu_1, \nu_2, \ldots, \nu_K$ the number of failed specimens detected at each voltage level for the investigated insulation subjected to accelerated life testing. The probability distribution function of failure times is postulated to belong to a very general class of functions defined by (55):

$$F(\delta, \epsilon) = \sum_{j=0}^{2} b_j c_j(t) \tag{50}$$

where δ and ϵ are shape and scale parameter. b_0, b_1, and b_2 have expressions which are functions of shape and scale parameters, as well as of the first and second moment of the distribution (55). The procedure for the derivation of the probability function of the failure times of the insulating material at a nominal (design) stress, V_E ($V_E < V_K$), $F(t_F, V_E)$, involves four steps. In the first step, the life data obtained at each test-voltage level are used to derive the distribution function from the family given by Eq. (50). Next, a predetermined number of quantiles, $q_1, q_2, \ldots, q_M$, are selected, and the corresponding values of times are obtained from each distribution; that is, for the distribution function corresponding to stress level s ($s = 1, \ldots, K$), $F(t_{FS}, V_S)$, failure times $t_{F1S}, t_{F2S}, \ldots, t_{FMS}$ are calculated. Then, a regression analysis is performed on these quantiles to obtain the corresponding quantiles at the nominal stress level, V_E. From the resulting quantiles, the target life distribution $F(t_F, V_E)$ is finally obtained through a suitable optimization process (55).

Accuracy and adaptability in life prediction can be coniugated to insulation characterization, realizing a compromise between nonparametric and parametric methods, resorting to the Kalman filter algorithm (56). It provides, indeed, a parametric but adaptive inference method which allows unbiased estimates of model parameters, particularly sensitive to the lowest test stresses, to be obtained. The Kalman filter algorithm can be applied to life models as follows.

First, a probabilistic life model which fits data from accelerated life tests, at least within narrow test-stress ranges, is chosen. Resorting to Eq. (5), it can be written as:

$$log t_{FP} = k' + k''\ f(S) + P/\beta \tag{51}$$

where P is a given value of failure probability.

Depending on the expression of $f(S)$, electrical, mechanical, and thermal life models (as well as multistress models) can be taken into account (57, 58). For example, $f(E) = E - E_H$ or $f(E) = \log(E/E_H)$ provide the exponential and inverse-power electrical life models [Eqs. (3) and (4)], respectively. Equation (51) collects the quantities to be estimated by the Kalman-filter procedure in order to characterize the investigated insulating material or system and infer design stresses. In fact, parameters k' and k'' are related to life line location and slope, while β depends on data dispersion.

The Kalman filter algorithm consists of observation and system equations which relate the observed quantities, for instance, failure times, and the system quantities, like the model parameters, calculated at each stress level. On the basis of Eq. (51), the observation and system equations can be written as (57)

$$log t_{FP_s} = [1 \ \ f(E_s)P][k'_s k''_s (1/\beta)_s]^T + v_s \tag{52}$$

$$[a_s b_s (1/\beta_s)]^T = G_s [a_{s-1} b_{s-1} (1/\beta)_{s-1}]^T + \Gamma_{s-1} w_{s-1} \tag{53}$$

where iteration s ($s = 1, \ldots, K$) corresponds to the sth life test; $s = 1$ and $s = K$ identify the accelerated life tests at the highest and lowest electrical stress levels of the test set, respectively, for a given temperature. v_s and w_{s-1} are observation and system errors, whose estimation has a fundamental role for the efficiency of the Kalman filter algorithm (57, 58), Γ_{s-1} is the error matrix, and G_s can be taken as coincident with the identity matrix for all s.

Since the Kalman filter algorithm is an iterative procedure which uses the estimates made at iteration $s-1$ to infer data at iteration s, its application to accelerated life testing is straightforward. At each test-stress level (iter-

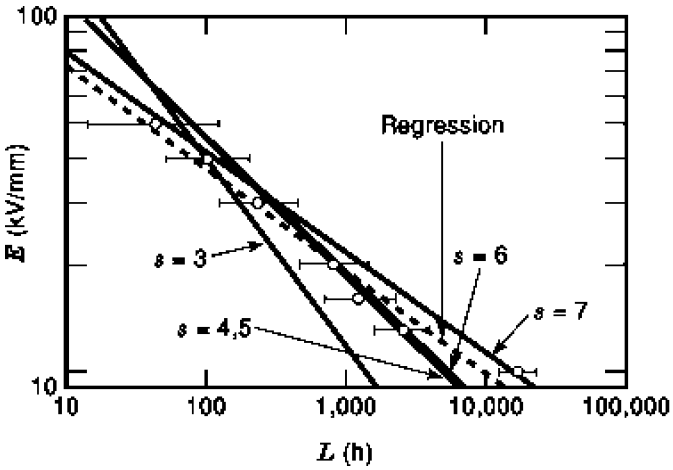

Figure 19. Application of the Kalman filter method to life data at probability 50% (confidence intervals at probability 90%) obtained from life tests performed on PET specimens at 110°C. The life lines obtained at each iteration (with $s \geq 3$) are displayed, together with the linear regression of all life data [after (57)].

ation), the updating and prediction relationships, derived from observation and system equations, are applied to estimate model parameters and to predict life at given probability and stress. Therefore, this method allows parameter estimation as well as life forecasting to be obtained, thus encompassing both parametric and nonparametric approaches dealt with above.

An advantage of the Kalman filter is that parameter estimates and life forecasting are particularly sensitive to the last iteration, that is, the lowest test-stress level considered, which is the closest to the expected operation stress. This feature is useful for those materials which show curvatures of the electrical life line, as those depicted in Fig. 19. As can be seen, deviation from the linear behavior of life points is detected by a Kalman filter, which adapts the assumed model (inverse-power in the figure) to fit the data recorded at each iteration with rate dependent on the uncertainty of the data; the larger data variance, the smaller the reaction of the Kalman filter to deviation of data from linearity [this result has been obtained by proper expressions of observation and system errors (57, 58)]. Of course, when life lines show clear tendency to a threshold, a more accurate description of endurance behavior can be obtained applying one of the threshold models described above.

BIBLIOGRAPHY

1. IEC 505-1, *Evaluation and Qualification of Electrical Insulation Systems*, 1991 (under revision).
2. L. Simoni, *Fundamentals of Endurance of Electrical Insulating Materials*, Bologna, Italy: CLUEB Publ., 1983.
3. L. Simoni, A new approach to the voltage endurance test on electrical insulation, *IEEE Trans. Electr. Insul.*, **8** (1): 76–86, 1973.
4. G. C. Montanari, L. Simoni, Aging phenomenology and modeling, *IEEE Trans. Electr. Insul.*, **28** (5): 755–776, 1993.
5. W. Nelson, *Applied Life Data Analysis*, New York: Wiley, 1982.
6. J. F. Lawless, *Statistical Models and Methods for Lifetime Data*, New York: Wiley, 1982.
7. J. C. Fothergill, Estimating the cumulative probability of failure data points to be plotted on the Weibull and other probability paper, *IEEE Trans. Electr. Insul.*, **25** (3): 89–492, 1990.
8. J. Jacquelin, A reliable algorithm for the exact mean rank function, *IEEE Trans. Electr. Insul.*, **28** (2): 168–171, 1993.
9. M. Cacciari, G. Mazzanti, G. C. Montanari, Comparison of maximum likelihood unbiasing methods for the estimation of the Weibull parameters, *IEEE Trans. Dielectr. Electr. Insul.*, **3** (1): 18–27, 1996.
10. G. C. Montanari *et al.*, Optimum Estimators for the Weibull Distribution for Data from Uncensored Tests, *IEEE Trans. Dielectr. Electr. Insul.*, **4** (3): 306–313, 1997.
11. G. C. Montanari, M. Cacciari, Electrical life threshold models for insulating materials subjected to electrical and multiple stresses. Part 2: probabilistic approach to generalized life models, *IEEE Trans. Electr. Insul.*, **27** (5): 987–999, 1992.
12. IEC243-1, Electric strength of insulating materials—Test methods Part 1: Tests of power frequencies, 1990.
13. T. W. Starr, H. S. Hendicott, A new accelerated approach to voltage endurance, *IEEE Trans. Power Appar. Syst.*, **80**: 515–522, 1961.
14. G. C. Montanari, M. Cacciari, Probabilistic modeling of insulating material endurance under constant and progressive-stress tests, *Metron*, **L** (1–2): 123–145, 1992.
15. T. Tanaka, A. Greenwood, *Advanced Power Cable Technology*, **1**, Boca Raton, FL: CRC Press, 1983.
16. C. Dang, J. L. Parpal, J. P. Crine, Electrical aging of extruded dielectric cables. Review of existing theories and data, *IEEE Trans. Dielectr. Electr. Insul.*, **3** (2): 237–247, 1996.
17. R. Bartnikas, R. J. Densley, R. M. Eichhorn, Long term accelerated aging tests on distribution cables under wet conditions, *IEEE Trans. Power Deliv.*, **11** (4): 1695–1699, 1996.
18. G. C. Montanari, Electrical life threshold models for insulating materials subjected to electrical and multiple stresses. Part 1: Investigation and comparison of life models, *IEEE Trans. Electr. Insul.*, **27** (5): 974–986, 1992.
19. G. Mazzanti, G. C. Montanari, A comparison between XLPE and EPR as insulating materials for HV cables, *IEEE Trans. Power Deliv.*, **12** (1): 15–28, 1997.
20. G. Bahder, T. W. Dakin, J. H. Lawson, Analysis of treeing type breakdown, CIGRE', paper n. 15.05, August 1976.
21. G. Bahder *et al.*, Physical model of electric aging and breakdown of extruded polymeric insulated power cables, *IEEE Trans. Power Appar. Syst.*, **101**: 1378–1388, 1982.
22. J. C. Fothergill, L. A. Dissado, P. J. Sweeney, A discharge-avalanche theory for the propagation of electrical trees. A physical basis for their voltage dependence, *IEEE Trans. Dielectr. Electr. Insul.*, **1** (3): 474–486, 1995.
23. G. C. Montanari, Aging and life models for insulation systems based on PD detection, *IEEE Trans. Dielectr. Electr. Insul.*, **2** (4): 667–675, 1995.
24. T. W. Dakin, S. A. Studniarz, *The voltage endurance of cast and molded resins*, *13th IEEE/NEMA EEI Conf.*, Boston, MA: 318–321, 1977.
25. IEC 216, *Guide for the Determination of Thermal Endurance Properties of Electrical Insulating Materials*, 1998.
26. J. P. Crine, Rate theory and polyethylene relaxation, *IEEE Trans. Electr. Insul.*, **22** (1): 169–174, 1986.

27. S. Glasstone, K. J. Laidler, H. Eyring, *The Theory of Rate Processes*, New York: McGraw Hill, 1941.
28. G. C. Montanari, G. Mazzanti, From thermodynamic to phenomenological multi-stress models for insulating materials without or with evidence of threshold, *J. Phys. D: Appl. Phys.*, **27**: 1691–1702, 1994.
29. L. Dissado, G. Mazzanti, G. C. Montanari, The role of trapped space charges in the electrical aging of insulating materials, *IEEE Trans. Dielectr. Electr. Insul.*, **5** (5): 496–506, 1997.
30. P. K. David, G. C. Montanari, Compensation effect in thermal aging investigated according to Eyring and Arrhenius models, *European Trans. Electr. Power Engin.*, **2** (3): 187–194, 1992.
31. J. P. Crine, A thermodynamic model for the compensation law and its physical significance for polymers, *J. Macromol. Sci.*, **23** (2): 201–219, 1984.
32. L. Dissado, G. Mazzanti, G. C. Montanari, The incorporation of space charge degradation in the life model for electric insulating materials, *IEEE Trans. Dielectr. Electr. Insul.*, **2** (6): 1147–1158, 1995.
33. L. Simoni, A general approach to the endurance of electrical insulation under temperature and voltage, *IEEE Trans. Electr. Insul.*, **16** (4): 277–289, 1981.
34. L. Simoni *et al.*, A general multi-stress life model for insulating materials with or without evidence of threshold, *IEEE Trans. Electr. Insul.*, **28** (3): 349–364, 1993.
35. T. W. Dakin, Electrical insulation deterioration treated as a chemical rate phenomenon, *AIEE Trans.*, **67**: 113–122, 1948.
36. T. W. Dakin, Electrical insulation deterioration, *Electrotechnology*, **3**: 129–130, 1960.
37. H. S. Hendicott, B. D. Hatch, R. G. Sohmer, Applications of the Eyring model to capacitor aging data, *IEEE Trans. Component Parts*, **12** (1): 34–41, 1965.
38. J. P. Crine, A. K. Vijh, A molecular approach to the physicochemical factors in the electric breakdown of polymers, *Appl. Phys. Communications*, **5**: 139–163, 1985.
39. J. P. Crine, J. L. Parpal, G. Lessard, A model of aging of dielectric extruded cables, *Proc. 3rd IEEE ICSD*, 347–351, 1989.
40. R. J. Densley, R. Bartnikas, B. Bernstein, Multiple-stress aging of solid dielectric extruded dry-cured insulation systems for power transmission cables, *IEEE PES Summer Meeting*, Vancouver, Canada, July 1993.
41. A. K. Jonscher, R. Lacoste, On a cumulative model of dielectric breakdown in solids, *IEEE Trans. Electr. Insul.*, **19** (6): 567–577, 1984.
42. L. A. Dissado, G. Mazzanti, G. C. Montanari," Elemental strain and trapped space charge in thermoelectrical aging of insulating materials. Part 1: elemental strain under thermo-electrical-mechanical stress", *IEEE Trans. Dielectr. Electr. Insul*, **8**(6), 959–965, 2001.
43. L. A. Dissado, G. Mazzanti, G. C. Montanari," Elemental strain and trapped space charge in thermoelectrical aging of insulating materials. Life modeling", *IEEE Trans. Dielectr. Electr. Insul*, **8**(6), 966–971, 2001.
44. G. Mazzanti, G. C. Montanari, L. A. Dissado," A space-charge life model for AC electrical aging of polymers", *IEEE Trans. Dielectr. Electr. Insul*, Vol.**6**, No. 6,pp. 864–875, December 1999.
45. G. Mazzanti, G. C. Montanari, L. Dissado," Electrical aging and life models: the role of space charge", *IEEE Transactions on Dielectrics and Electrical Insulation*, Vol.**12**,pp. 876–890, October 2005.
46. A. Cavallini, D. Fabiani, G. Mazzanti, G. C. Montanari," A life model based on space charge quantities for HVDC polymeric cables subjected to voltage polarity inversions", *IEEE Trans. Dielectr. Electr. Insul*, Vol.**9**, No. 4,pp. 514–523, August 2002.
47. G. Mazzanti, G. C. Montanari, S. Serra," Aging model of Polyethylene-based materials for HV cables founded on damage inception and growth from air-filled voids", *IEEE ICSD*, pp. 525–529, Toulose, France, July 2004.
48. G. Mazzanti, G. C. Montanari, S. Serra," Theory of inception mechanism and growth of defect-induced damage in Polyethylene cable insulation", *J. Appl. Phys.*, Vol.**98**, No. 3, pp. 034102.1–034102.15, August 2005.
49. G. Jiang, J. Kuang, S. Boggs," Critical parameters for electrical tree formation in XLPE", *IEEE Trans. Pow. Del.*, Vol.**13**, no. 2,pp. 292–296, April 1998.
50. G. C. Montanari, A comparative investigation of electrothermal endurance models for insulating materials and systems characterization, *IEEE Electr. Insul. Magaz.*, **13**, 1997.
51. S. N. Zhurkov, Kinetic concept of the strength of solids, *Int. J. Fract. Mech.*, **1**: 311–323, 1965.
52. EPRI Report TR-100268, *Multistress aging of extruded insulation systems for transmission cables*, 1992.
53. J. P. Crine, The compensation law revisited: Application to dielectric aging, *IEEE Trans. Electr. Insul.*, **26** (4): 811–818, 1991.
54. G. Mazzanti *et al.*, Combined electro-thermal-mechanical model for life prediction of electrical insulating materials, *Proc. IEEE CEIDP*, Virginia Beach, USA, 274–277, October 1995.
55. J. Biernat *et al.*, Reliability considerations in accelerated life testing of electrical insulation with generalized life distribution function, *IEEE Trans. Power Syst.*, **7** (2): 656–664, 1992.
56. R. E. Kalman, A new approach to linear filtering and prediction problems, *Trans. ASME, series D, Journal of Basic Engineering*, **82**: 35–45, 1960.
57. G. C. Montanari *et al.*, Application of Kalman filter for electrical endurance characterization of insulating materials and systems, *IEEE Trans. Dielectr. Electr. Insul.*, **3** (1): 56–63, 1996.
58. M. Cacciari, G. C. Montanari, C. P. Barry, Thermal endurance of electrical insulating materials studied by the use of the Kalman filter, *European Trans. Electr. Power Engin.*, **6** (2): 103–110, 1996.

GIAN CARLO MONTANARI
GIOVANNI MAZZANTI
University of Bologna, Italy